Clays and Clay Minerals, Vol. 44, No. 2, 244–256, 1996.

WEATHERING OF CHLORITE IN A QUARTZ-CHLORITE SCHIST: I. MINERALOGICAL AND CHEMICAL CHANGES

TAKASHI MURAKAMI,†[1] HIROSHI ISOBE,[2] TSUTOMU SATO,[2] AND TOSHIHIKO OHNUKI[2]

[1] Department of Earth Sciences, Faculty of Science, Ehime University, Matsuyama, Ehime 790, Japan

[2] Department of Environmental Safety Research, Japan Atomic Energy Research Institute, Tokai, Ibaraki 319-11, Japan

Abstract—The weathering of chlorite, one of the major minerals of the host rock in the uranium ore deposit at Koongarra, Australia, was examined by X-ray diffraction (XRD) analysis, scanning electron microscopy (SEM), electron microprobe analysis, and transmission electron microscopy (TEM). The conversion sequence of chlorite weathering is: (1) chlorite; (2) chlorite/vermiculite intergrade (showing XRD responses to various treatments intermediate between those of chlorite and vermiculite); (3) interstratified chlorite and vermiculite; (4) vermiculite; and (5) kaolinite. This sequence may be more simply expressed as chlorite → vermiculite → kaolinite. The weathering finally changed chlorite into sub-micrometer to micrometer sized Fe minerals and kaolinite. The transformation of chlorite to vermiculite is chemically characterized by an Fe and Mg loss with a slight decrease in the Al/Si ratio. Mg continues to be released throughout the weathering. Fe minerals formed through chlorite weathering are located between chlorite and vermiculite domains (a few μm in size) at first, and then accumulated between grain boundaries, occasionally forming veins. The distribution of Fe minerals is suggestive of preferential pathways of water movement. The time-dependent nature of mineral alteration demonstrated in the present study must be taken into account for the quantitative estimation of radionuclide migration.

Key Words—Alteration, Chlorite, Kaolinite, Uranium Ore Deposit, Vermiculite, Weathering.

INTRODUCTION

The disposal of high level radioactive waste is now a worldwide concern, involving a variety of scientific fields such as physics, chemistry, geology and biology. Radioactive waste is proposed to be disposed of in rocks at a depth of several hundred meters below the Earth's surface since it has high radioactivity that will persist for a long time. The most probable pathway for the waste to be transported to the Earth's surface is migration through ground water, which also reacts with the host rocks. By water-rock interactions such as weathering, the rock-forming minerals are changed structurally and chemically with time, and the attainment of equilibrium may be delayed or never reached (Dibble and Tiller 1981). The reactions may take longer than the time specified during the safety assessment of high level waste disposal. Actinides, a major concern because of their long-lasting radioactivity, may flow from the source and react with then-coexisting minerals of the surrounding rock, which vary with time as a function of the weathering mechanisms and kinetics. Radionuclide migration is affected by mineral weathering (Murakami et al. 1991a; Murakami et al. 1992) and the effects have been quantitatively estimated (Ohnuki et al. 1991; Murakami and Kimura 1993; Ohnuki et al. 1993).

The Koongarra uranium ore deposit in the Northern Territory, Australia, is one of the sites for natural analogue studies of radionuclide migration (Airey 1986; Airey and Ivanovich 1986). The ore deposit exists just below the surface to 60 m deep in a tropical monsoon area. The quartz-chlorite schist, host rock, has been subjected to weathering for more than one million years (Airey et al. 1986). Although quartz is resistant to weathering and persists even at the surface, chlorite has been weathered to clay minerals and Fe minerals (Airey 1985). Figure 1 schematically shows a cross section at Koongarra (modified from Snelling 1980). The secondary uranium ore deposit, uranyl phosphate and dispersed uranium zones (Figure 1), which has been formed by weathering of the primary ore deposit and the precipitation of secondary uranium minerals, is located in the weathered zone which is present from the surface down to approximately 20 m. Uranium is found as uranium phosphates in the secondary ore deposit and it is associated with the weathering products of chlorite downstream from the secondary ore deposit (Snelling 1980). The latter case is similar to the radionuclide migration which may follow the disposal of high level radioactive waste and continue over geologic time. Details of geology at Koongarra are summarized elsewhere (Snelling 1992).

Vermiculite, smectite, kaolinite, goethite and hematite are observed, resulting from the weathering of chlorite, in the Alligator Rivers region where Koongarra is a district (Airey 1985). The existence of vermiculite, smectite, kaolinite and goethite sug-

† Present address: Mineralogical Institute, Graduate School of Science, The University of Tokyo, Hongo, Bunkyo-ku, Tokyo 113, Japan.

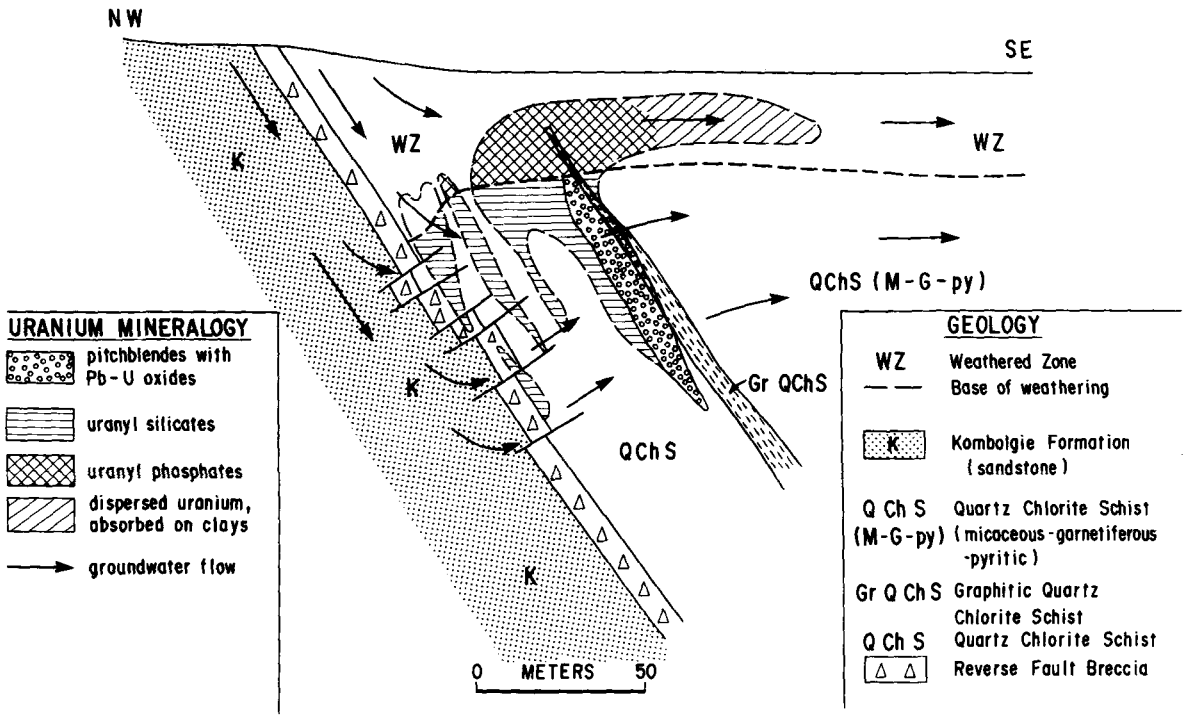

Figure 1. Schematic representation of the geological and mineralogical cross section at Koongarra (modified from Snelling 1980).

gests that the weathering of chlorite begins with vermiculitization. Vermiculitization is associated with the oxidation of ferrous ions and a loss of Fe and Mg (Gilkes and Little 1972). More recently, the vermiculitization process has been found to be more complicated. Chlorite is altered to regularly interstratified chlorite/vermiculite, followed by irregularly interstratified chlorite/vermiculite and then vermiculite (Herbillon and Makumbi 1975). Ross (1975) and Ross and Kodama (1976) pointed out from their experimental results that oxidation of the structural Fe^{2+} is essential in the alteration of chlorite, and chlorites having different Fe^{2+} contents may react differently under the same weathering conditions. Conversely, Proust et al. (1986) insisted that vermiculitization proceeds by the release of ferrous ions from the 2:1 layers, and is associated with the release of Mg ions from the hydroxide sheets but not by the oxidation of ferrous ions. Different solid alteration products have been identified in the

Table 1. List of the samples used for the present study.

Sample name[1]	Description	Methods[2]
DDH3-10.9	Weathered, with schist texture	XRD, SEM, EMPA
DDH3-17.5	Weathered, with schist texture	XRD
DDH3-18.9	Weathered, with schist texture	XRD, SEM, EMPA
DDH3-20.6	Intermediately weathered	XRD, SEM, EMPA
DDH3-22.0	Intermediately weathered	XRD
DDH3-24.1	Slightly weathered	XRD, SEM, EMPA
DDH3-24.5	Slightly weathered	XRD
DDH3-25.9	Unweathered	XRD, SEM, EMPA
DDH3-28.0	Unweathered	XRD, SEM, EMPA
DDH3-33.4	Unweathered	XRD, SEM, EMPA, TEM
DDH4-7.7	Weathered, with schist texture	EMPA
DDH4-23.3	Intermediately weathered	SEM, EMPA
DDH4-23.6	Intermediately weathered	SEM, EMPA, TEM
PH58-2.3	Weathered, without schist texture	XRD, SEM, EMPA

[1] Sample name combines a core hole name and depth from surface in meters.
[2] Analytical techniques applied for samples: EMPA-electron probe microanalysis; SEM-scanning electron microscopy; TEM-transmission electron microscopy; and XRD-X-ray diffraction analysis.

https://doi.org/10.1346/CCMN.1996.0440210 Published online by Cambridge University Press

Table 2. Compositions of chlorite, interstratified chlorite/vermiculite and vermiculite along the DDH3 core hole.[1]

	Chlorite													
	Chamosite										Clinochlore			
Depth (m)	33.4	33.4	33.4	28.0	28.0	25.9	25.9	25.9	Average	σ	33.4	33.4	33.4	28.0
SiO_2 (wt.%)	27.5	27.5	28.7	26.9	27.0	26.2	26.5	25.8	27.0	0.9	28.8	29.3	29.2	29.9
Al_2O_3	18.5	20.9	19.3	18.5	18.9	19.2	18.9	19.9	19.3	0.8	22.9	23.0	21.5	19.9
TiO_2	0.9	0.0	0.0	0.0	0.0	0.0	0.0	0.2	0.1	0.3	0.0	0.1	0.1	0.0
FeO[2]	27.8	25.8	27.6	25.5	25.1	28.2	28.4	28.9	27.1	1.5	15.8	14.3	16.1	11.2
MnO	0.3	0.3	0.4	0.4	0.4	0.5	0.6	0.4	0.4	0.1	0.4	0.2	0.1	0.0
MgO	12.3	12.8	11.8	16.3	16.4	13.5	13.5	12.7	13.7	1.8	19.6	21.2	20.5	25.2
K_2O	0.1	0.0	0.1	0.0	0.0	0.0	0.0	0.0	0.0	0.0	0.0	0.0	0.0	0.0
$H_2O_{cal.}$[3]	11.2	11.4	11.4	11.3	11.4	11.2	11.2	11.2	11.3	0.1	12.1	12.2	12.1	12.2
Total	98.5	98.8	99.2	98.9	99.3	98.7	98.9	99.2	98.9	0.3	99.6	100.3	99.7	98.4
Cation numbers based on $O_{10}(OH)_8$														
Si	2.94	2.90	3.03	2.84	2.84	2.81	2.84	2.77	2.87	0.08	2.86	2.86	2.91	2.95
Al	1.06	1.10	0.97	1.16	1.16	1.19	1.16	1.23	1.13	0.08	1.14	1.14	1.09	1.05
Σ tet.	4.00	4.00	4.00	4.00	4.00	4.00	4.00	4.00	4.00	0.00	4.00	4.00	4.00	4.00
Al	1.27	1.50	1.44	1.15	1.18	1.24	1.22	1.28	1.28	0.12	1.55	1.51	1.43	1.27
Ti	0.07	0.00	0.00	0.00	0.00	0.00	0.00	0.02	0.01	0.03	0.00	0.01	0.01	0.00
Fe^{2+}	2.48	2.27	2.43	2.25	2.21	2.53	2.54	2.59	2.41	0.15	1.32	1.17	1.34	0.92
Mn	0.03	0.03	0.03	0.03	0.04	0.05	0.05	0.04	0.04	0.01	0.03	0.02	0.01	0.00
Mg	1.96	2.01	1.85	2.57	2.57	2.16	2.15	2.03	2.16	0.27	2.90	3.10	3.03	3.71
Σ oct.	5.82	5.80	5.76	6.00	5.99	5.97	5.97	5.96	5.91	0.10	5.80	5.80	5.82	5.89
K	0.01	0.00	0.01	0.00	0.00	0.00	0.00	0.00	0.00	0.01	0.00	0.00	0.00	0.00

	Mixture of chlorite/vermiculite[4]									Vermiculite[7]	
	W. chamosite[5]				W. clinochlore[5]					W. chamosite[5]	
Depth(m)	24.1	24.1	24.1	24.1	24.1	24.1	24.1	24.1	Depth (m)	20.6	20.6
SiO_2 (wt.%)	37.3	34.7	36.6	35.3	37.3	34.1	39.0	34.5	SiO_2 (wt.%)	38.1	37.7
Al_2O_3	20.9	19.9	21.2	22.2	26.6	21.2	22.5	20.2	Al_2O_3	24.2	25.0
TiO_2	0.8	1.3	0.2	0.0	0.0	0.0	0.8	0.0	TiO_2	0.2	0.2
Fe_2O_3[2]	14.6	18.1	17.5	17.7	7.7	13.3	13.3	16.5	Fe_2O_3[2]	12.1	12.1
MnO	0.1	0.0	0.0	0.1	0.0	0.0	0.0	0.2	MnO	0.2	0.1
MgO	12.0	12.3	10.6	11.7	13.9	18.6	11.0	15.6	MgO	11.8	11.5
K_2O	0.6	0.5	0.2	0.2	0.5	0.0	0.6	0.0	K_2O	0.0	0.1
Total[6]	86.3	86.9	86.2	87.1	86.0	87.3	87.2	87.0	Total[6]	86.5	86.6
									Cation numbers based on $O_{10}(OH)_2$		
									Si	2.78	2.75
									Al	1.22	1.25
									Σ tet.	4.00	4.00
									Al	0.87	0.90
									Ti	0.01	0.01
									Fe^{3+}	0.67	0.67
									Mn	0.01	0.01
									Mg	0.88	0.85
									Σ oct.	2.43	2.43
									K	0.00	0.01
									Mg	0.40	0.40

[1] Na and Ca were not detected.
[2] All Fe as FeO for chlorite and as Fe_2O_3 for mixture of chlorite/vermiculite and vermiculite.
[3] Calculated based on $O_{10}(OH)_8$.
[4] Mixture of chlorite/vermiculite contains chlorite, chlorite/vermiculite intergrade, and interstratified chlorite/vermiculite.
[5] W. chamosite represents weathered products of chamosite and W. clinochlore represents weathered products of clinochlore.
[6] Totals without H_2O.
[7] Interlayer charge is assumed to be 0.8 (see text for explanation).

late stage of chlorite weathering: kaolinite through nontronite (Herbillon and Makumbi 1975); vermiculite and goethite (Ross et al. 1982); kaolinite, Fe oxides and smectite (Proust et al. 1987); and Fe^{3+}-rich smectite (Buurman et al. 1988). In the present study, the process of chlorite weathering will be elucidated with emphasis on changes in mineral assemblages, textures and compositions.

https://doi.org/10.1346/CCMN.1996.0440210 Published online by Cambridge University Press

Table 2. Extended.

Clinochlore					
28.0	25.9	25.9	25.9	Average	σ
29.8	29.9	29.8	30.0	29.6	0.4
20.2	19.9	19.0	19.7	20.8	1.5
0.0	0.0	0.2	0.1	0.1	0.1
12.0	11.2	14.2	12.6	13.4	2.0
0.0	0.0	0.2	0.0	0.1	0.1
24.7	25.2	24.4	24.6	23.2	2.3
0.0	0.0	0.0	0.0	0.0	0.0
12.2	12.2	12.1	12.2	12.1	0.1
98.9	98.4	99.9	99.1	99.3	0.7
Cation numbers based on $O_{10}(OH)_8$					
2.94	2.95	2.95	2.96	2.92	0.04
1.06	1.05	1.05	1.04	1.08	0.04
4.00	4.00	4.00	4.00	4.00	0.00
1.29	1.27	1.16	1.24	1.34	0.14
0.00	0.00	0.01	0.01	0.00	0.01
0.98	0.92	1.18	1.04	1.11	0.17
0.00	0.00	0.01	0.00	0.01	0.01
3.62	3.71	3.58	3.61	3.41	0.33
5.89	5.89	5.94	5.89	5.87	0.05
0.00	0.00	0.00	0.00	0.00	0.00

Vermiculite[7]				
W. clinochlore[5]				
20.6	20.6	20.6	Average	σ
38.0	40.8	40.5	39.0	1.5
25.2	26.7	28.9	26.0	1.9
0.2	0.0	0.1	0.1	0.1
11.6	10.2	8.1	10.8	1.7
0.1	0.2	0.1	0.1	0.1
11.8	8.7	7.8	10.3	1.9
0.2	0.1	0.1	0.1	0.1
87.0	86.6	85.5	86.4	0.5
Cation numbers based on $O_{10}(OH)_2$				
2.76	2.92	2.91	2.83	0.09
1.24	1.08	1.09	1.17	0.09
4.00	4.00	4.00	4.00	0.00
0.91	1.18	1.36	1.04	0.22
0.01	0.00	0.00	0.01	0.01
0.63	0.55	0.44	0.59	0.10
0.00	0.01	0.01	0.01	0.00
0.88	0.53	0.43	0.71	0.22
2.44	2.27	2.24	2.36	0.10
0.01	0.01	0.00	0.01	0.01
0.39	0.40	0.40	0.40	0.00

EXPERIMENTAL

Samples

The samples from Koongarra and the analytical techniques applied are listed in Table 1. The diamond drill holes (DDH) were all drilled at an inclination of approximately 50° so as to intersect the mineralization perpendicular to the schistosity. The exploration percussion holes (PH) were also drilled. The sample names comprise the corehole name and the vertical depth from the surface in meters, for example, DDH3-33.4.

X-ray Diffraction Analysis (XRD)

XRD studies were made of randomly oriented specimens to examine mineral species in bulk samples and on oriented specimens to facilitate clay mineral identifications. For the oriented specimens, the bulk samples were powdered to fine grains and then centrifuged after suspension in water to obtain clay fractions less than 2 μm in size. The bulk and oriented specimens were analyzed with graphite-monochromatized CuKα at 35 kV and 15 mA or 40 kV and 20 mA. The diffractometer was calibrated using silicon as an external standard.

Heat treatment and cation-saturation methods were used for the identification of the clay minerals. With the heat treatment method, XRD intensities were collected from oriented, air-dried specimens and from the same specimens treated with ethylene glycol. Data collection was repeated after heating the specimens at 450°C for 1.5 h. XRD intensities were collected for some specimens after heating them at 600°C for 1.5 h. With the cation saturation method, the interlayer cations of the specimens were exchanged by Mg^{2+} and K^+ ions. With glycerol treatment after each cation exchange, chlorite, vermiculite and smectite were distinguished from each other by their characteristic peak positions.

Scanning Electron Microscopy (SEM) and Electron Microprobe Analysis (EMPA)

Polished thin sections were observed by light microscopy to roughly understand the mineralogical characteristics of the specimens. After the observations, the specimens were coated with carbon by vacuum evaporation for SEM and EMPA studies. A Hitachi S-650 scanning electron microscope equipped with a Kevex 7000Q energy dispersive X-ray analysis system was used for the SEM and EMPA studies. Because polished, thin sections were used, backscattered electron imaging (BEI) was mostly employed for the SEM studies. The operating voltage was 20 kV and the beam current was 0.1 nA for the EMPA studies. The effective beam size during the operation was 2–3 μm. The standards used were: Na, albite; Mg, periclase; Al, corundum; Si, quartz; K, orthoclase; Ca, wollastonite; Ti, rutile; Mn, spessartine; and Fe, hematite. ZAF correction (Kevex software) was made for differential matrix effects. For the present analyses, two standard deviations, that is 2σ for Mg, Al, Si and Fe were less than 0.4 wt% and those for Na, K, Ca, Ti and Mn, less than 0.1 wt%. The structural formulas were calculated based on $O_{10}(OH)_8$ for chlorite and $O_{10}(OH)_2$ for vermiculite.

Transmission Electron Microscopy (TEM)

Disk specimens of 3 mm in diameter were drilled out from some of the thin sections and ion-thinned for

https://doi.org/10.1346/CCMN.1996.0440210 Published online by Cambridge University Press

Figure 2. TEM image of chlorite showing lath-like domains.

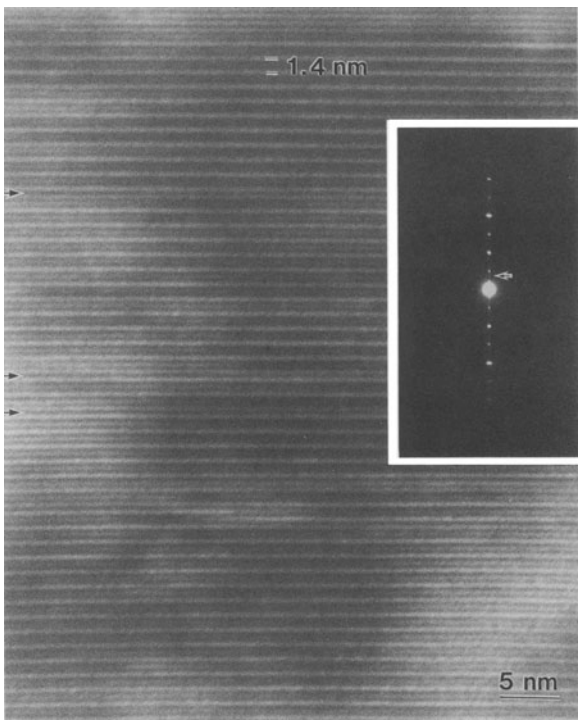

Figure 3. HRTEM image of chlorite and its corresponding electron diffraction pattern showing stacking disorder of chlorite. The thick arrows demonstrate stacking faults, and the inset arrow indicates a diffuse streak.

the TEM studies. The ion-thinning method was carried out with a Gatan dual ion mill with a liquid nitrogen cooling cold stage to avoid heat damage of the specimens. The TEM examination was completed on a JEOL 2000FX. High resolution transmission electron microscopy (HRTEM) was employed by using multiple-beam bright field imaging.

RESULTS

Characteristics of Chlorite

EMPA studies (Table 2) and BEI observations revealed that there are two kinds of chlorites at Koongarra: 1) Fe-rich chlorite; and 2) Mg-rich chlorite. The Fe-rich chlorite is 50-to-300 μm in size and the Mg-rich chlorite is 20–80 μm in size. The Fe-rich chlorite corresponds to chamosite and the Mg-rich is a clinochlore (Newman and Brown 1987). The XRD intensity ratios of 1.4 to 0.7 nm peaks of chlorite in DDH3 and DDH4 cores indicate that chamosite is predominant over clinochlore (Wilson 1987).

TEM studies of the chamosite grains revealed that each grain of a few tenth mm is not a single crystal but consists of lath-like domains of 10-to-100 nm width, normal to the c^* axis, and 100-to-1000 nm in length (Figure 2). The domains are attached to each other with the c^* axis in common or share low angle grain boundaries.

Under appropriate HRTEM conditions, the TOT layers can be imaged as broad fringes, the hydroxide sheets as narrower dark fringes, and sites between them as white fringes (Iijima and Buseck 1978; Veblen 1983; Eggleton and Banfield 1985). Figure 3 shows a sequence of chlorite layers normal to the c^* axis by HRTEM. The contrast is reversed compared to that under the appropriate conditions. The white fringes between pairs of the dark fringes correspond to the TOT layers and the gray fringes in pairs of the dark fringes correspond to the hydroxide sheets. There is stacking disorder in chlorite domains, which results in slightly diffuse streaks in an electron diffraction pattern (for example, Figure 3 an inset arrow). Stacking faults are shown by thick arrows in the HRTEM image (Figure 3). Because the contrast is reversed in Figure 3 and the faults are located between the TOT layers, the faults are interpreted as interlayers without the hydroxide sheets. This means that the interlayers without the hydroxide sheets are those of biotite layers that survived the retrograde chloritization in the Alligator Rivers region (Page et al. 1980).

Weathered Products

A series of XRD patterns of the clay minerals in the DDH3 samples is presented in Figure 4. The spec-

https://doi.org/10.1346/CCMN.1996.0440210 Published online by Cambridge University Press

imens cover the whole range of the chlorite weathering. Figure 4a indicates the possible existence of chlorite, vermiculite, mica and kaolinite for all specimens except for DDH3-18.9 which is mainly kaolinite. Quartz is identified in every specimen. Micaceous minerals (peaks at 1.0 nm) are not always found in the specimens (for example, DDH3-25.9 in Figure 4a).

The XRD patterns show no significant change in ethylene glycol solvation except for that of DDH3-20.6, but, upon heating to 450°C, the XRD patterns change significantly (Figure 4). After heating the specimens at 450°C, the 1.4 nm peak is present in DDH3-33.4, -25.9 and -24.5, and in DDH3-24.1, although it was very weak in intensity, but it was absent in DDH3-22.0 and shallower specimens (Figure 4b). The presence and absence of the 1.4 nm peak upon heating corresponded exactly to the presence and absence of chlorite.

VERMICULITE. The 1.4 nm peaks in DDH3-22.0 and -20.6 are attributed to vermiculite because of the disappearance of the 1.4 nm peaks upon heating to 450°C and the peak shift after K-saturation and glycerol solvation. Because the peak at 1.4 nm of DDH3-22.0 was not shifted by Mg-saturation and glycerol solvation and it was shifted to 1.0–1.1 nm by K-saturation and glycerol solvation, the vermiculite is estimated to have a layer charge of 0.7–0.8 e.s.u./half unit cell (Suquet et al. 1977).

KAOLINITE. The 0.7 nm peaks persist after the disappearance of 1.4 nm peaks upon heating to 450°C for DDH3-22.0, -20.6 and -18.9 (Figure 4b), indicating that kaolinite is present at a depth of 22.0 and shallower. The small peak at 0.7 nm remaining on heating to 450°C for DDH3-24.1 (Figure 5) is attributed to chlorite. These suggest that kaolinite begins to form at a depth between 22 and 24 m.

CHLORITE/VERMICULITE INTERGRADE. The peak at 1.4 nm of DDH3-24.1 appearing on K-saturation and glycerol solvation was first considered to be that of chlorite (Figure 5, shorter-tailed arrow). If the chlorite had had the same characteristics of the primary chlorite, the peak at 1.4 nm would have remained after heating to 450°C. However, a smaller peak at 1.4 nm remained after heating, than that after K-saturation and glycerol solvation (Figure 5). This suggests that a phase other than chlorite contributes to the peak at 1.4 nm. This phase behaves as chlorite upon K-saturation and glycerol solvation and as vermiculite upon heating, indicating that the phase is chlorite/vermiculite intergrade (Wilson 1987). Sample DDH3-24.5 showed the same responses to the treatments as those of DDH3-24.1. In addition to the increase in intensity at 1.0-to-1.1 nm, the decrease in the intensity ratio of the 1.4/0.7 nm peaks upon heating to 450°C is greater than those for DDH3-33.4 and -25.9, which contain chlorite but not its weathered products. The intensity ratio of the 1.4/0.7 nm peaks upon K-saturation and glycerol solvation is similar to that on Mg-saturation and glycerol solvation. Thus, DDH3-24.5 contains chlorite/vermiculite intergrade as well as chlorite.

INTERSTRATIFIED CHLORITE/VERMICULITE. The peak appearing upon K-saturation and glycerol solvation shown by a longer-tailed arrow in Figure 5 suggests the presence of a phase other than chlorite or vermiculite. Because chlorite/vermiculite interstratified minerals have been often observed (Herbillon and Makumbi 1975), an XRD theoretical profile of interstratified chlorite/vermiculite was calculated by the method given by Kakinoki and Komura (1952) and Watanabe et al. (1974), and compared to the observed profile (Figure 5). The calculated profile fit the observed one best when it was assumed that the ratio of chlorite:vermiculite (including chlorite/vermiculite intergrade) was 3:7, and that the interstratified chlorite/vermiculite had a randomly interstratified structure. Therefore, the phase shown by the longer-tailed arrow in Figure 5 is interstratified chlorite/vermiculite with 0.3 chlorite and 0.7 vermiculite. The calculation also showed that the presence of interstratified chlorite/vermiculite justified the high intensity ratio of 1.4/0.7 nm peaks on Mg-saturation and glycerol solvation (Figure 5). Broad peaks at 1.2 nm of DDH3-24.1 and -22.0 appeared upon heating (arrows in Figure 4b) also support the evidence of the presence of interstratified chlorite/vermiculite (Johnson 1964). Thus, DDH3-24.1 is unique, it contains chlorite (Figure 5, a small peak at 1.4 nm upon heating to 450°C), chlorite/vermiculite intergrade and interstratified chlorite/vermiculite. The high intensity ratio of 1.4/0.7 nm peaks after Mg-saturation and glycerol solvation and the low intensities at 1.4 nm peaks after K-saturation and glycerol solvation and upon heating to 450°C, suggests that the major phase of DDH3-24.1 is interstratified chlorite/vermiculite, and that chlorite and chlorite/vermiculite intergrade are minor.

OTHER MINERALS. Goethite and hematite were also found in the weathered zone in addition to kaolinite. Goethite occurred from the bottom of the weathered zone to the surface. A Mössbauer study revealed the presence of ferrihydrite (Edis et al. 1992) that is difficult to be detected by XRD.

A peak profile change of DDH3-20.6 was observed upon Mg-saturation and ethylene glycol solvation as shown in Figure 6 where the 1.4 nm peak of the air-dried sample was changed to form a 1.4 nm peak with less intensity accompanied by a shoulder at a lower angle by ethylene glycol. This fact indicates that part of the 1.4 nm peak of the air-dried sample is attributed to smectite.

Chemical Analyses of Weathered Products

The composition of minerals analyzed by EMPA are listed in Table 2. The kaolinite grains were too small

https://doi.org/10.1346/CCMN.1996.0440210 Published online by Cambridge University Press

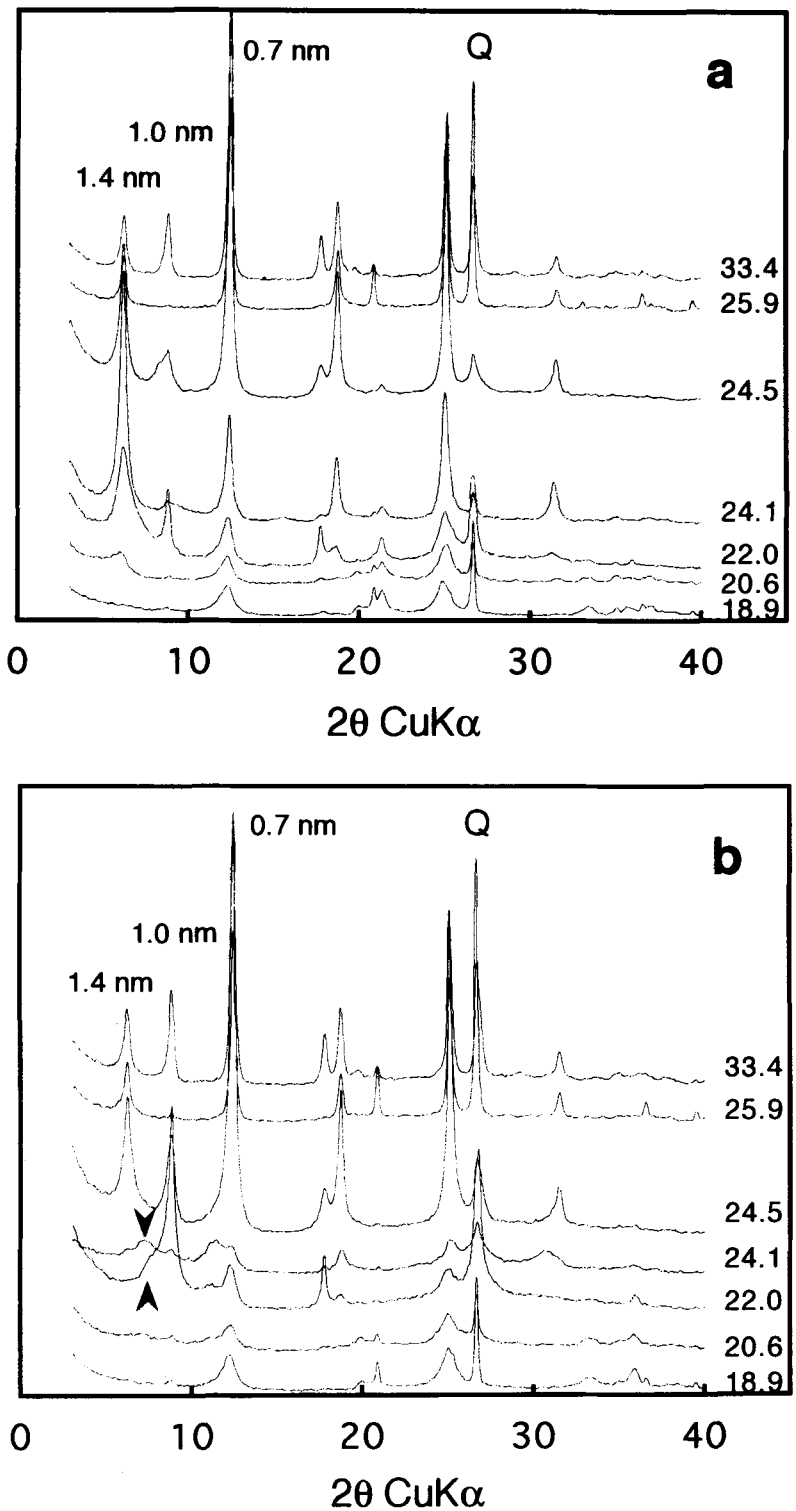

Figure 4. X-ray diffractograms of a suite from the DDH3 core: a) oriented and air-dried; and b) oriented after heating at 450°C. The numbers on the right indicate depths from the surface in meters. Q denotes quartz. The arrows show 1.2-nm peaks.

https://doi.org/10.1346/CCMN.1996.0440210 Published online by Cambridge University Press

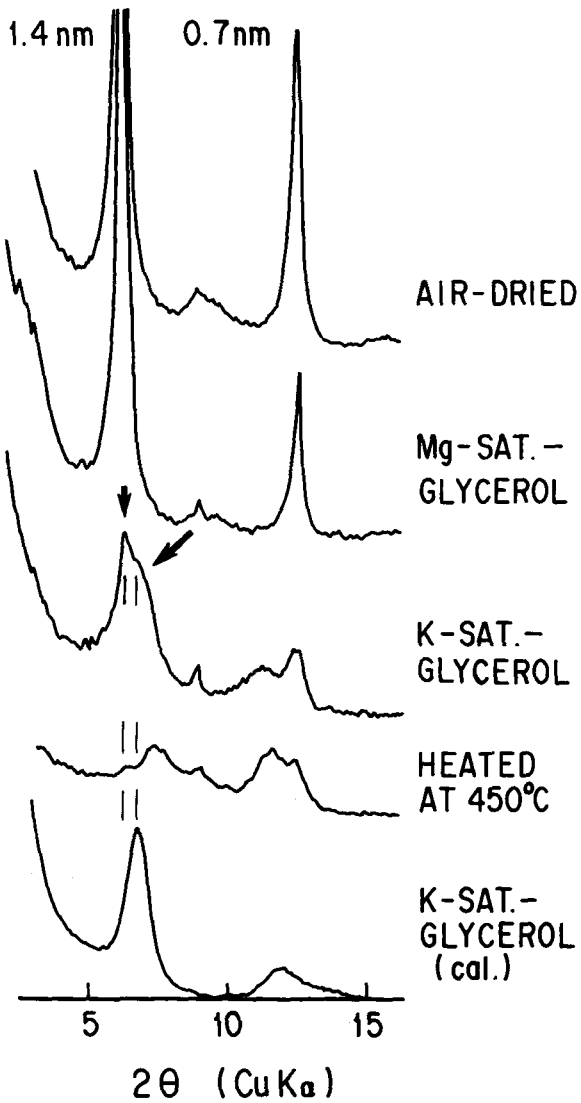

Figure 5. X-ray diffractograms of DDH3-24.1. XRD theoretical profile of interstratified chlorite (30%) and vermiculite (70%) is compared. The shorter-tailed arrow indicates the presence of chlorite. The longer-tailed arrow indicates the presence of interstratified chlorite and vermiculite. The decrease in intensity at 1.4 nm after heat treatment compared with that on K-saturation and glycerol solvation indicates the presence of chlorite/vermiculite intergrade.

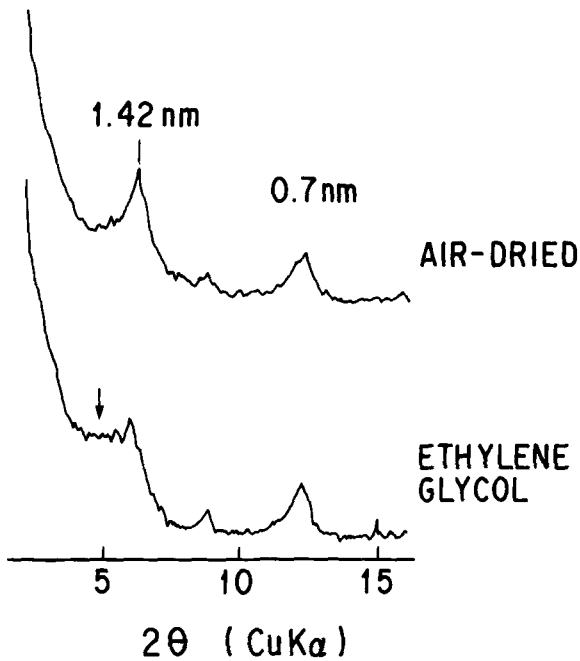

Figure 6. X-ray diffractograms of DDH3-20.6. The shoulder indicated by the arrow suggests the presence of smectite.

in size to be analyzed by EMPA, and they are not listed.

Because the XRD results revealed that vermiculite has a layer charge of 0.7-to-0.8, the cation numbers in vermiculite were calculated assuming a layer charge of 0.8. The analyses of vermiculite show that the vermiculite is intermediate between dioctahedral and trioctahedral (2.2-to-2.5 for octahedral cations per $O_{10}(OH)_2$ in Table 2). This conclusion is also supported by the XRD results: the (060) reflections of DDH3-24.1 and -20.6 indicate that both have peaks at 0.154 nm and broad ones at 0.149 nm with broad shoulders between the two peaks. A similar observation was made by Ross et al. (1982). Because DDH3-20.6 contains kaolinite, there must be kaolinite contributed to the peak at 0.149 nm of DDH3-20.6.

During the conversion of chlorite to vermiculite, the numbers of Si and Al ions do not change significantly while those of Fe and Mg ions decrease significantly (Table 2). The mole ratios of Fe and Mg to total cations were calculated in order to clearly understand the decrease in Fe and Mg cations with weathering. The mole numbers of the cations were calculated based on the data in Table 2. The range from 20-to-25 m corresponds to the transition zone where chlorite is weathered to kaolinite. In the conversion, the Fe mole fraction in weathered chamosite decreases significantly while that in weathered clinochlore slightly decreases (Figure 7a). Conversely, the Mg mole fraction in weathered clinochlore decreases significantly while that in weathered chamosite slightly decreases (Figure 7b). At the final stage of vermiculitization, the Fe/Mg mole ratio is similar to weathered chamosite and clinochlore (see "vermiculite" in Table 2). The analyses of the samples in the last two columns of weathered clinochlore ("vermiculite" in Table 2) are the Fe- and Mg-poorest ones for vermiculite in the present study. These may be the most weathered vermiculite.

Fe released during the conversion of chlorite to vermiculite may be consumed to form ferrihydrite, goethite and hematite, the Fe minerals abundant in the weathered zone. Because Mg is only found as an im-

https://doi.org/10.1346/CCMN.1996.0440210 Published online by Cambridge University Press

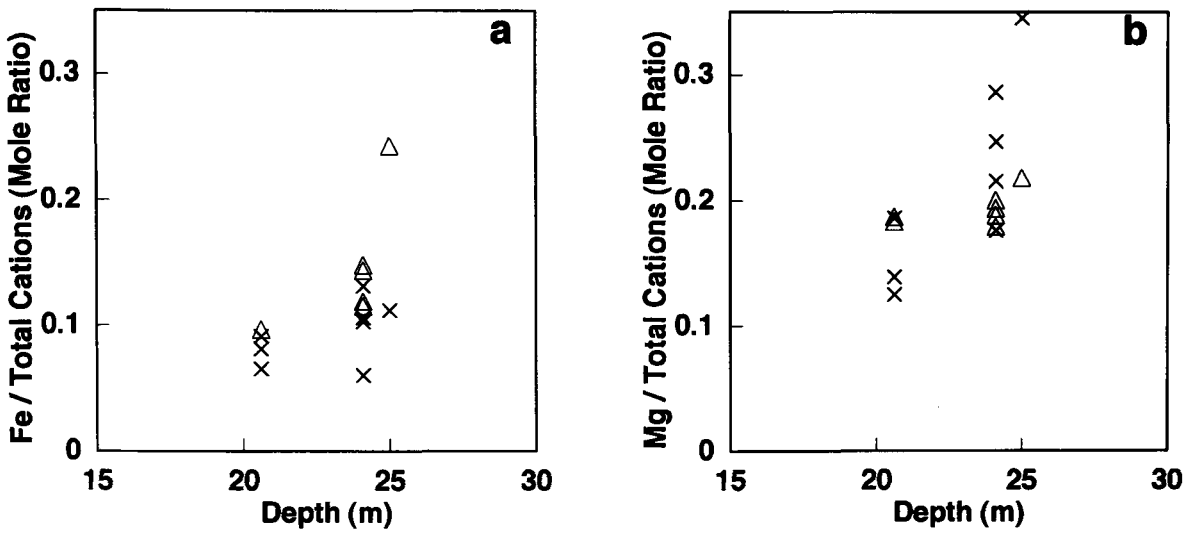

Figure 7. Variations in mole ratios of Fe (a) and Mg (b) to total cations with weathering. Triangles represent the variations for chamosite and crosses for clinochlore. The values at 25 m are averages of chamosite and clinochlore in the unweathered zone.

purity of kaolinite in the weathered zone, most of the Mg released during the conversion dissolves into ground water.

Textures of Weathered Rocks

The unweathered samples have a schistose texture with alternating parallel quartz and chlorite grains. The chamosite and clinochlore are distinct not only in size, but also in contrast of the BEI micrograph, the latter is much darker (Figure 8a). Figure 8b indicates that a partially weathered chamosite (sample DDH3-24.1 from the transition zone between the unweathered and weathered zone in Figure 1) is chemically inhomogeneous and has a layer texture with alternating white and gray contrast containing precipitates of Fe minerals (brightest areas). The XRD results revealed that DDH3-24.1 contains chlorite, chlorite/vermiculite intergrade, and interstratified chlorite/vermiculite. The Fe content in chamosite is greater than that in vermiculite by about 15 wt% (Table 2, as oxide forms), suggesting chamosite is brighter in contrast of BEI micrographs than vermiculite. Therefore, the alternating white and gray contrast probably correspond to chamosite-rich and vermiculite-rich domains, respectively. The Fe mineral precipitates are often found between chamosite-rich and vermiculite-rich domains of slightly weathered chamosite grains (Figure 8b, smaller, straight arrow). They are accumulated in the weathered chamosite as weathering progresses (Figure 8b, larger, straight arrow). The occurrence of Fe minerals suggests that Fe precipitates as Fe minerals soon after the Fe is released from chamosite by weathering.

Figure 8c shows the Fe mineral distribution in sample DDH4-23.3 from an intensely weathered part next to a fracture (Figure 8c, top), to an intermediately weathered part (Figure 8c, middle and bottom). The degree of weathering of an area is less and less as the area is distant from the fracture. Fe minerals are dominant with scattered quartz grains (Figure 8c, massive, gray in contrast at the upper part) in the intensely weathered part where clay minerals are also abundant (Figure 8d, gray in contrast). In the middle of Figure 8c, Fe minerals are seen to occur at grain boundaries of quartz (massive, gray in contrast). Veins consisting of mainly Fe minerals are often found in the weathered samples.

Figure 8c shows how weathering propagates along a fracture. The schistosity in Figure 8c is parallel to the fracture. Fine-grained Fe and clay minerals (Figure 8d white and gray areas, respectively) along with quartz (Figure 8d, black area) are found near the fracture as found in the weathered zone while the original texture is still preserved at the bottom (Figure 8c). The degree of weathering indicates that the weathering started at the fracture and then progressed vertically to the fracture toward the bottom of the section, especially at grain boundaries. When fractures intersect schistosities, weathering is found to progress along the schistosities. The weathering propagation along fractures mentioned above was observed in the transition zone. When the weathering along fractures is completed, vermiculite disappears and the weathered zone appears. Fractures were also observed in the unweathered zone, generally without weathering.

Coarse-grained, weathered products are not seen but Fe minerals and clay minerals (probably kaolinite by XRD) of sub micrometers in size are dominant as well as quartz in the weathered zone. The original schistose

https://doi.org/10.1346/CCMN.1996.0440210 Published online by Cambridge University Press

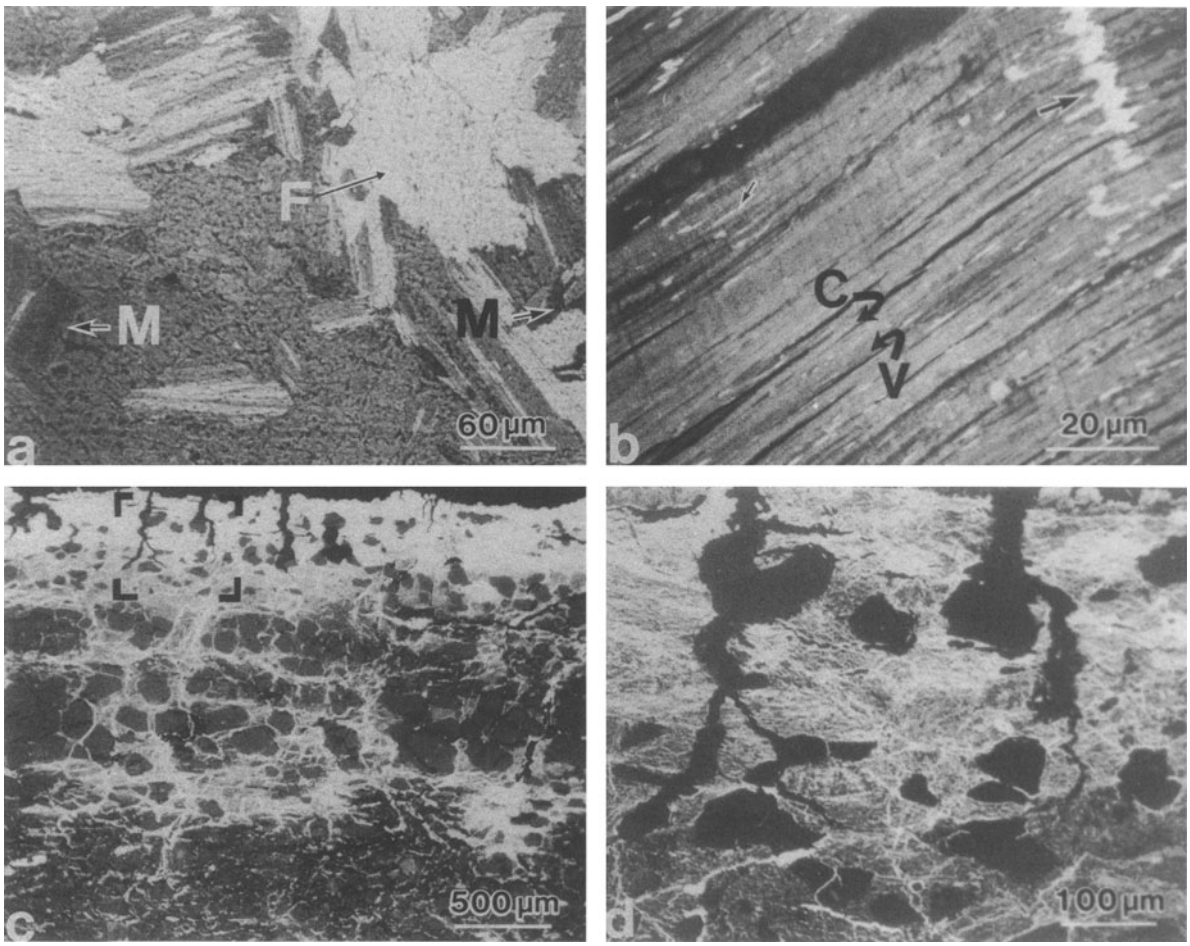

Figure 8. Backscattered electron images showing: (a) chamosite or Fe-rich chlorite (denoted by F), and clinochlore or Mg-rich chlorite (M) in an unweathered rock (sample DDH3-33.4); (b) Fe mineral precipitates (straight arrows), and chamosite-rich (denoted by C) and vermiculite-rich domains (denoted by V), in a weathered chamosite (sample DDH3-24.1); (c) Fe mineral distribution (brightest areas) in a weathered rock (sample DDH4-23.3); and (d) enlargement of the area shown by the marks in (c).

texture is retained up to 8 m depth but not retained at 2.3 m depth.

DISCUSSION

The XRD results are summarized as follows, the conversion sequence for the layer silicates from chlorite to kaolinite is: (1) chlorite; (2) chlorite/vermiculite intergrade; (3) interstratified chlorite/vermiculite; (4) vermiculite; and (5) kaolinite. The formation of chlorite/vermiculite intergrade may be due to the incomplete transformation from chlorite to vermiculite. Vermiculite occurring during the conversion is intermediate between dioctahedral and trioctahedral. Smectite was found only in sample DDH3-20.6, which also contained vermiculite and kaolinite. Some studies reported that smectite occurs as a weathered product (Herbillon and Makumbi 1975; Proust et al. 1987; Buurman et al. 1988). Although smectite could occur during the conversion of vermiculite to kaolinite, the lifetime of the smectite must be short compared with that of vermiculite.

The conversion sequence may be more simply expressed as chlorite → vermiculite → kaolinite. On the basis of the XRD results, the presence of the clay minerals can be described as a function of depth. Chlorite, which is not weathered even at 26 m in depth from the surface vertically, rapidly decreases between 25 and 24 m in depth, and disappears at 23 m. Vermiculite appears at 25 m depth and kaolinite begins to persist at 23 m depth. Vermiculite disappears at 20 m where kaolinite is predominant as it is in the shallower zone. The vermiculite-present zone corresponds to the transition zone where weathering was observed to propagate along fractures.

The Fe mole fraction in weathered chamosite decreases significantly while the Mg mole fraction de-

https://doi.org/10.1346/CCMN.1996.0440210 Published online by Cambridge University Press

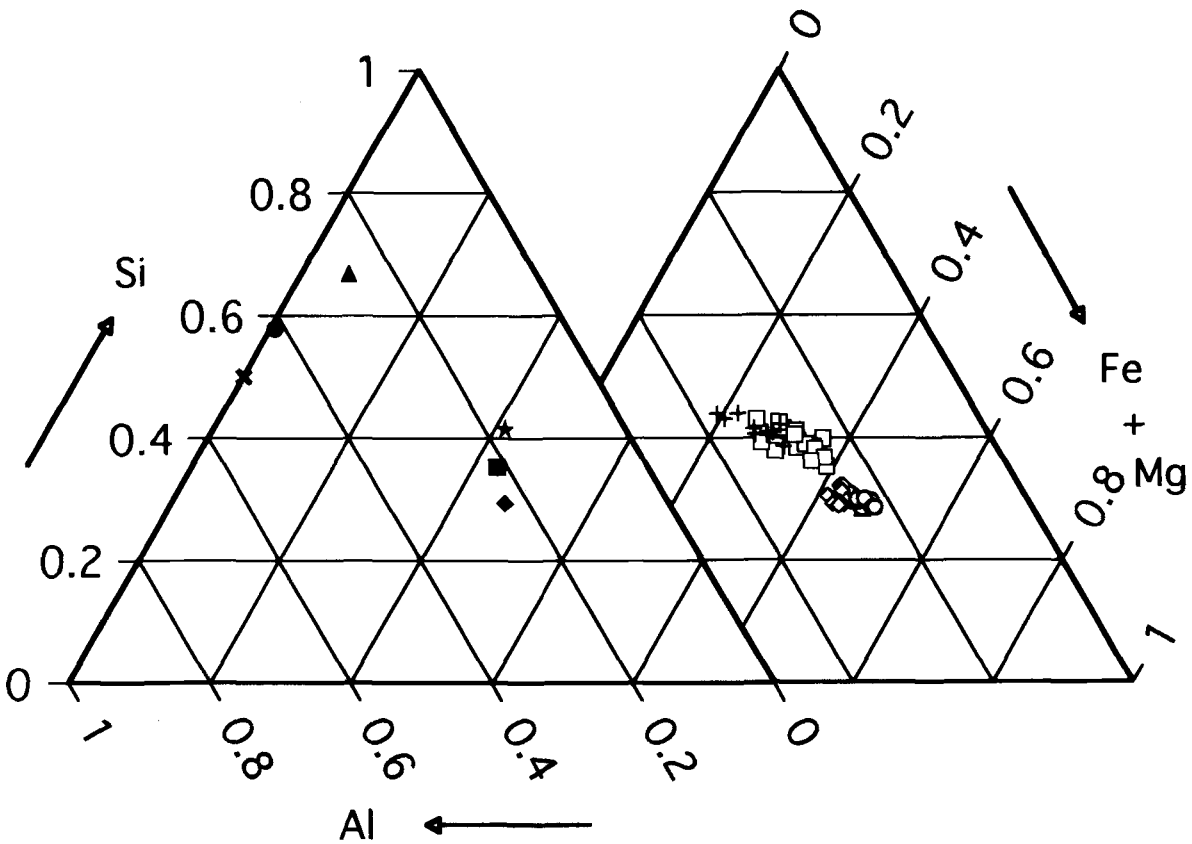

Figure 9. Plots of atomic proportion of Si, Al (total) and (Fe + Mg) for chlorites, mixture of chlorite and vermiculite, and vermiculites on the right, and for some reference minerals on the left. The plots in the right figure are based on the EMPA analyses. Legend: Open diamonds (◇) chlorites of DDH3-33.4; open triangles (△) chlorites of DDH3-28.0; open circles (○) chlorites of DDH3-25.9; open squares (□) mixture of chlorite and vermiculite of DDH3-24.1; pluses (+) vermiculites of DDH3-20.6; solid diamond (◆) chlorite (Ross and Kodama 1976); solid square (■) interstratified chlorite/vermiculite (Ross and Kodama 1976); solid star (★) trioctahedral vermiculite (Newman and Brown 1987); solid triangle (▲) montmorillonite (Foster 1953); solid circle (●) beidellite (Weir 1965); and cross (X) kaolinite with ideal composition.

creases slightly (Figure 7). Conversely, the Fe mole fraction in weathered clinochlore decreases slightly while the Mg mole fraction decreases significantly (Figure 7). Ross and Kodama (1976) suggested that the difference in Fe content of chlorite affects vermiculitization of chlorite. However, the present results indicate that chamosite and clinochlore are similarly weathered in terms of chemical composition. The compositions of vermiculites at the final stage of vermiculitization are similar to one another even if their starting chlorites are different in Fe and Mg contents (Table 2). These suggest that the Fe and Mg contents play a similar role in vermiculitization.

The change in ratios of Si:Al(total):(Fe + Mg) with vermiculitization is shown in Figure 9 along with the ratios of reference minerals. The vermiculitization is characterized by a significant Fe and Mg loss with a slight decrease in the Al/Si ratio with progress in weathering. The results by Ross and Kodama (1976) show that the compositional change from chlorite (solid diamond in Figure 9) to interstratified chlorite/vermiculite (solid square) approximately falls into a line of the change from chlorite to normal trioctahedral vermiculite (solid star). On the other hand, chlorite in the present study (open diamonds, triangles and circles) apparently changes its composition toward that of kaolinite (cross) or beidellite (solid circle), but not that of montmorillonite (solid triangle) or normal trioctahedral vermiculite (solid star). The compositional change progresses through a mixture of chlorite/vermiculite (open squares) including chlorite, chlorite/vermiculite intergrade and interstratified chlorite/vermiculite. The change in the ratio of Si, Al and (Fe + Mg) and the decrease in total octahedral cation numbers (Table 2) with progress in weathering suggests that vermiculite forms as trioctahedral first and becomes dioctahedral by losing octahedral cations with progress in weathering. This is consistent with the presence of an intermediate trioctahedral-dioctahedral structure of vermiculite (Ross et al. 1982) and a di-

https://doi.org/10.1346/CCMN.1996.0440210 Published online by Cambridge University Press

octahedral one (Proust 1982) by chlorite weathering reported previously.

The conversion from chlorite to vermiculite probably occurs layer-by-layer because the morphology of chlorite grains remains during vermiculitization and the grains of weathered chlorite have a layer texture with alternating chlorite-rich and vermiculite-rich domains. Fe released during the transformation forms Fe minerals which are distributed between chlorite and vermiculite domains as sub-micrometer size grains, and then accumulated within the host grains. But, the formation mechanism of kaolinite is ambiguous, no evidence for transformation or precipitation was found. Although the kaolinite grains were too small in size to be analyzed by EMPA, the composition of kaolinite may be similar to an ideal kaolinite composition (Newman and Brown 1987). Thus, Fe is again released during the formation of kaolinite, forming Fe minerals which are distributed at grain boundaries and fractures. The additional accumulation of Fe minerals during the formation of kaolinite was confirmed by chemical analysis (Murakami et al. 1991b). The Fe mineral distribution in a rock is suggestive of water pathways. Most of Mg released by the chlorite weathering is leached away from the system because the weathered products contain much less Mg than chlorite. This is consistent with a high Mg content (about 20 ppm) in ground water (Payne et al. 1992).

ACKNOWLEDGMENTS

The authors are indebted to Mr. P. Duerden of the Australian Nuclear Science and Technology Organization and Dr. A. A. Snelling for the assistance in the sample collection; Dr. K. L. Smith of the Australian Nuclear Science and Technology Organization and Mr. K. Fukai of Japan Atomic Energy Research Institute for the use of JEOL 2000FX electron microscopes. We thank Mr. P. Duerden for the review of an early version of the manuscript. We are also grateful to Dr. Y. Kobayashi, Dr. K. Sekine and Mr. N. Yanase of Japan Atomic Energy Research Institute for the discussions and encouragement throughout this study. To Drs. E. Essene, R. E. Ferrell, Jr. and R. A. Eggleton for their careful reviews and corrections.

REFERENCES

Airey PL. 1985. Radionuclide migration around uranium ore bodies—Analogue of radioactive waste repositories. Annual Report 1983-1984, AAEC/C45. United States Nuclear Regulatory Commission Contract NRC-04-81-172. Sydney: Australian Nuclear Science and Technology Organisation. 142p.

Airey PL. 1986. Radionuclide migration around uranium ore bodies in the Alligator Rivers Region of the Northern Territory of Australia—Analogue of radioactive waste repositories—a review. Chem Geol 55:255–268.

Airey PL, Golian C, Lever DA. 1986. An approach to the mathematical modelling of the uranium series redistribution within ore bodies. Topical Report AAEC/C49. Sydney: Australian Nuclear Science and Technology Organisation. 106p.

Airey PL, Ivanovich M. 1986. Geochemical analogues of high-level radioactive waste repositories. Chem Geol 55: 203–213.

Buurman P, Meijer EL, van Wijck JH. 1988. Weathering of chlorite and vermiculite in ultramafic rocks of Cabo Ortegal, northwestern Spain. Clays & Clay Miner 36:263–269.

Dibble Jr WE, Tiller WA. 1981. Kinetic model of zeolite paragenesis in tuffaceous sediments. Clays & Clay Miner 29:323–330.

Edis R, Cao L, Cashion J, Klessa D, Koppi AJ, Murakami T, Nightingale T, Payne T, Snelling A, Yanase N. 1992. Chemistry and mineralogy of rocks and soils, Alligator Rivers Analogue Project Final Report Vol. 8. Sydney: Australian Nuclear Science and Technology Organisation. DOE/HMIP/PR/92/078. 255p.

Eggleton RA, Banfield JF. 1985. The alteration of granitic biotite to chlorite. Am Mineral 70:902–910.

Foster MD. 1953. Geochemical studies of clay minerals. II. Relation between ionic substitution and swelling in montmorillonite. Am Mineral 38:994–1006.

Gilkes RJ, Little IP. 1972. Weathering of chlorite and some associations of trace elements in Permian phyllites in southeast Queensland. Geoderma 7:233–247.

Herbillon AJ, Makumbi MN. 1975. Weathering of chlorite in a soil derived from a chlorite-schist under humid tropical conditions. Geoderma 13:89–104.

Iijima S, Buseck PR. 1978. Experimental study of disordered mica structures by high-resolution electron microscopy. Acta Crystal A34:709–719.

Johnson LJ. 1964. Occurrence of regularly interstratified chlorite-vermiculite as a weathering product of chlorite in a soil. Am Mineral 49:556–572.

Kakinoki J, Komura Y. 1952. Intensity of X-ray by a one-dimensionally disordered crystal. J Phys Soc Japan 7:30–35.

Murakami T, Isobe H, Edis R. 1991a. Effects of chlorite alteration on uranium redistribution in Koongarra, Australia. In:Abrajano Jr T, Johnson LH, editors. Mat Res Soc Symp Proc (Scientific Basis for Nuclear Waste Management XIV). Pittsburgh, PA: The Materials Research Society. 212:741–748.

Murakami T, Isobe H, Nagano T, Nakashima S. 1992. Uranium redistribution and fixation during chlorite alteration at Koongarra, Australia. In:Sombret CG, editor. Mat Res Soc Symp Proc (Scientific Basis for Nuclear Waste Management XV). Pittsburgh, PA: The Materials Research Society. 257:473–480.

Murakami T, Kimura H. 1993. A modelling study of the effect of rock alteration on the redistribution of uranium. In:Interrante CG, Pabalan RT, editors. Mat Res Soc Symp Proc (Scientific Basis for Nuclear Waste Management XVI). Pittsburgh, PA: The Materials Research Society. 294: 535–542.

Murakami T, Ohnuki T, Sato T. 1991b. Kinetic analysis of chlorite alteration. Abstracts for Fall Meeting of Mineralogical Society of Japan. Japan:Sendai. p. 50.

Newman ACD, Brown G. 1987. The chemical constitution of clays. In:Newman ACD, editor. Chemistry of Clays and Clay Minerals. Essex, UK:Longman Scientific & Technical. 1–128.

Ohnuki T, Watanabe S, Murakami T. 1991. Study on role of Th-234 in uranium series nuclides migration. In:Abrajano Jr T, Johnson LH, editors. Mat Res Soc Symp Proc (Scientific Basis for Nuclear Waste Management XIV). Pittsburgh, PA: The Materials Research Society. 212:733–740.

Ohnuki T, Murakami T, Yanase N. 1993. A modelling study on the fractionation of uranium between minerals by rock alteration. In:Interrante CG, Pabalan RT, editors. Mat Res Soc Symp Proc (Scientific Basis for Nuclear Waste Man-

agement XVI). Pittsburgh, PA: The Materials Research Society. 294:527–533.

Page RW, Compston W, Needham RS. 1980. Geochronology and evolution of the late-Archaean basement and Proterozoic rocks in the Alligator Rivers uranium field, Northern Territory, Australia. In:Ferguson J, Goleby AB, editors. Proceedings of the IAEA International Uranium Symposium in the Pine Creek Geosyncline. Vienna: IAEA. 39–68.

Payne T, Edis R, Herczeg A, Sekine K, Seo T, Waite D, Yanase N. 1992. Groundwater chemistry, Alligator Rivers Analogue Project Final Report. 7. Sydney: Australian Nuclear Science and Technology Organisation. DOE/HMIP/PR/92/077. 185p.

Proust D. 1982. Supergene alteration of metamorphic chlorite in an amphibolite from Massif Central, France. Clay Mineral 17:159–173.

Proust D, Dudoignon P, Bouchet A, Meunier A. 1987. Marine and supergene alteration progresses in a chloritized amphibole-schist, Deux-Serves, France. Clay Mineral 22: 129–143.

Proust D, Eymery J-P, Beaufort D. 1986. Supergene vermiculitization of a magnesian chlorite: iron and magnesium removal processes. Clays & Clay Miner 34:572–580.

Ross GJ. 1975. Experimental alteration of chlorites into vermiculites by chemical oxidation. Nature 255:133–134.

Ross GJ, Kodama H. 1976. Experimental alteration of a chlorite into a regularly interstratified chlorite-vermiculite by chemical oxidation. Clays & Clay Miner 24:183–190.

Ross GJ, Wang C, Ozken AI, Rees HW. 1982. Weathering of chlorite and mica in a New Brunswick podzol developed on till derived from chlorite-mica schist. Geoderma 27: 255–267.

Snelling AA. 1980. Uraninite and its alteration products, Koongarra uranium deposit. In: Ferguson J, Goleby AB, editors. Proceedings of the IAEA International Symposium Uranium in the Pine Creek Geosyncline. Vienna: IAEA. 487–498.

Snelling AA. 1992. Geologic setting: Alligator Rivers Analogue Project Final Report. Vol. 2. Sydney: Australian Nuclear Science and Technology Organisation. DOE/HMIP/PR/92/072. 118p.

Suquet H, Iiyama JT, Kodama H, Pezerat H. 1977. Synthesis and swelling properties of saponites with increasing layer charge. Clays & Clay Miner 25:231–242.

Veblen DR. 1983. Microstructure and mixed layering in intergrown wonesite, chlorite, talc, biotite, and kaolinite. Am Mineral 68:566–580.

Watanabe T, Nakamuta Y, Shirozu H. 1974. An interstratified mineral of chlorite and saponite from the Wanibuchi mine. J Mineral Soc Jpn 11:123–130 (in Japanese).

Weir AH. 1965. Potassium retention in montmorillonite. Clay Miner 6:17–22.

Wilson MJ. 1987. X-ray powder diffraction methods. In: Wilson MJ, editor. A Handbook of Determinative Methods in Clay Mineralogy. New York:Chapman and Hall. 26–98.

(Received 12 November 1993; accepted 31 July 1995; Ms. 2438)